

Short Communication

## Prediction of Corrosion Rates of Ni-TiN composite coating using a Radial Basis Function Neural Network

Yan Liu\*, Xingguo Han, Li Kang\*, Qiang Li

School of Energy and Building Environment, Guilin University of Aerospace Technology, Guilin, 541004, China

\*E-mail: [2019009@guat.edu.cn](mailto:2019009@guat.edu.cn) and [liudm109@163.com](mailto:liudm109@163.com)

Received: 18 February 2022 / Accepted: 26 March 2022 / Published: 7 May 2022

---

In this work a radial basis function (RBF) neural network was used for predicting the corrosion rate in Ni-TiN composite coatings that were deposited via pulse electrode deposition onto the surface of T8 steel. The surface morphology and phase composition of the coatings before and after corrosion were investigated by atomic force microscopy (AFM), scanning electron microscopy (SEM), and X-ray diffraction (XRD). The results show that the RBF neural network had a 3×4×1 structure. The maximum and minimum errors of this neural network were 2.28% and 0.04%, respectively. An optimum flat, fine, and compact microstructure was detected for Ni-TiN composite coatings manufactured with a TiN concentration of 9 g/L, a bath temperature of 45°C, and a current density of 0.6 A/dm<sup>2</sup>. Ni-TiN composite coatings obtained by using the parameters mentioned in serial number 1 manifested the strongest corrosion with a corrosion potential as high as -0.925 V. Whereas, Ni-TiN composite coatings deposited using the parameters mentioned in Serial number 9, demonstrated the lowest corrosion rate, indicating an outstanding corrosion resistance.

---

**Keywords:** RBF neural network; Ni-TiN composite coating; Corrosion rate; Prediction

### 1. INTRODUCTION

It is generally accepted that metal-based ceramics composite nanocoatings manifest a high hardness, excellent wear resistance, and corrosion resistance, and thus, outperform Ni-based coatings [1-4]. Therefore, such metal-based ceramic composite nanocoatings have attracted considerable research interest recently. Xia *et al.* [5] successfully prefabricated Ni-TiN coatings by using an electrodeposition method, where the corresponding coatings exhibited a surface hardness of ~34.5 GPa. Ma *et al.* [6] studied the preparation procedure of Ni-AlN coatings. They found that hardness as high as 767.9 HV can be achieved for the coating by adopting a pulse electrodeposition technique. Zhu *et al.* [7] showed that RE-Ni-W-P-SiC coatings can be deposited by applying the electrodeposition technique. Their

results revealed that the deposition rate was primarily determined by the duty ratio and the pulse frequency. In our previous study, we utilized a backward propagation model for calculating the microhardness of Ni-TiN coatings [8]. This work is based on the prediction of the corrosion rates of Ni-TiN composite coatings by using a radial basis function model.

RBF (Radial basis function) neural networks are efficient feed-forward neural networks, which possess a simple structure and fast training speed. At present, RBF neural networks have been applied to predict the performance of nanocoatings by utilizing their self-learning function, associative storage function, and their capability to rapidly search for the optimal solution. For instance, Liu *et al.* [9] reported that the performance of Fe-Cu coatings can be successfully predicted using an RBF neural network. They discovered that the sputtering time had little influence on the properties of the coating. Yuan *et al.* [10] applied the RBF neural network for calculating the deposition efficiency of metal coatings. Their results indicated that the RBF neural network could predict the deposition efficiency rather accurately.

Although many studies on metal-based ceramic composite nanocoatings and the use of RBF neural networks have been published, there are only a few reports concerning the prediction of the corrosion rates of Ni-TiN composite coatings by using RBF neural networks. The novelties of this work can be summarized as follows: (1) A RBF neural network was established for predicting the corrosion rates of Ni-TiN composite coatings. (2) The orthogonal experimental data were used for establishing the RBF neural network model. (3) The prediction errors of this RBF model have also been discussed in this work. In addition, the surface morphology and phase composition of the coatings before and after corrosion were analyzed by scanning electron microscopy (SEM), X-ray diffractometer (XRD), and electrochemical measurements.

## 2. EXPERIMENTAL

### 2.1 Preparation

T8 steel substrates with a size of 20mm×10mm×2mm were used as the cathode. Pure nickel plates with a size of 20mm×20mm×2mm were employed as the anode. Before electroplating, the T8 steel substrate and Ni plates were polished using 200, 400, 600, and 800 sandpapers, respectively. Next, the T8 steel substrate and Ni plates were disposed of for the removal of oil and activation. Finally, the Ni-TiN composite coatings were deposited by pulsed-current electrodeposition onto the surface of the T8 steel substrates. The parameters concerning the chemical and plating processes for the prefabrication of the Ni-TiN composite coatings have been shown in Table 1.

**Table 1.** Reagents and plating parameters for prefabricating Ni-TiN composite coatings.

Reagents	Parameters
NiSO <sub>4</sub> ·6H <sub>2</sub> O	250 g/L
NiCl <sub>2</sub> ·6H <sub>2</sub> O	30 g/L
H <sub>3</sub> BO <sub>3</sub>	20 g/L
C <sub>12</sub> H <sub>25</sub> SO <sub>4</sub> Na	0.1 g/L
TiN concentration	3~12 g/L
Electrolyte temperature	45~60°C
Duty cycle	50%
Current density	0.2~0.8 A/dm <sup>2</sup>
Plating time	45 min

## 2.2 Corrosion experiment

The samples coated with Ni-TiN composite were corroded in a 2.5% NaCl solution at 25°C for 2 h. Afterward, the samples were rinsed with distilled water and acetone. The corrosion losses of the Ni-TiN composite coatings were weighed by using an XSE105 microelectronic balance (precision 0.01 mg), and the corrosion rates were calculated according to Equation (1).

$$V = \frac{M}{S \times T} \quad (1)$$

where  $V$  represents the corrosion rate of the coating (mg/(mm<sup>2</sup>·h)),  $M$  represents the corrosion loss (mg),  $S$  represents the surface area of the coatings (mm<sup>2</sup>), and  $T$  represents the corrosion time (h).

The surface structure and corrosion morphology of the Ni-TiN composite coatings were analyzed by scanning electron microscope (SEM, S3400), and the phase composition was determined by X-ray diffractometer (XRD, XRD-7000).

The electrochemical corrosion characteristics of Ni-TiN composite coatings were measured using a CS350 electrochemical instrument (Wuhan Corrtest Instrument Co., Ltd, China) in a 0.4 M NaCl solution at room temperature. A three-electrode system was used, with a saturated calomel electrode (SCE) acting as the reference electrode, the platinum plate acting as the auxiliary electrode, and the Ni-TiN composite coatings acting as the working electrode. Potentiodynamic polarization curves were collected under a corrosion potential of 2 V to -2 V at a scanning rate of 1 mV/s.

## 2.3 Orthogonal experiment

It had been reported previously that the TiN concentration, electrolyte temperature, and current density generally have a significant influence on the corrosion rates of Ni-TiN composite coatings [11]. Therefore, these parameters were selected as the main factors for the design of an orthogonal experiment. A L<sub>9</sub>(4<sup>3</sup>) table was chosen as the orthogonal experiment table according to the conventional orthogonal design [12]. The experimental results for the deposition of Ni-TiN composite coatings have been shown in Table 2.

**Table 2.** Results of orthogonal experiment

Serial number	TiN concentration (g·L <sup>-1</sup> )	Electrolyte temperature (°C)	Current density (A·dm <sup>-2</sup> )
1	3	45	0.2
2	3	50	0.4
3	3	55	0.6
4	3	60	0.8
5	6	45	0.4
6	6	50	0.2
7	6	55	0.8
8	6	60	0.6
9	9	45	0.6
10	9	50	0.8
11	9	55	0.2
12	9	60	0.4
13	12	45	0.8
14	12	50	0.6
15	12	55	0.4
16	12	60	0.2

### 3. RESULTS AND DISCUSSION

#### 3.1 Establishment of the RBF neural network

RBF neural networks have been reported to exhibit excellent performance in terms of the approximation and global optimal characteristics [13]. The structure of the RBF neural network is displayed in Fig. 1. The RBF neural network used in this work consisted of three layers: an input layer, a hidden layer, and an output layer.

The TiN particle concentration, bath temperature, and current density were taken as the input layer of the RBF neural network, whereas the corrosion rate of the Ni-TiN composite coatings was taken as the output layer.

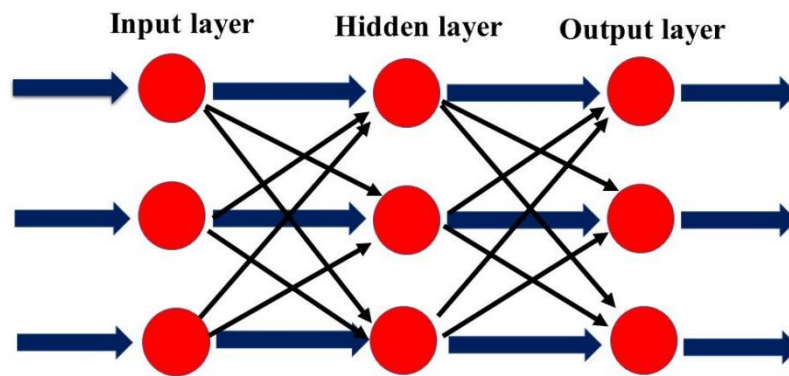


**Figure 1.** Schematic diagram of the RBF neural network

### 3.2 Training process of the RBF neural network

The training process of the RBF neural network is described as follows: First, the data in Table 2 were normalized using Equation (2). Secondly, the `traindxdn` function was employed as the training function, and the linear function was taken as the hidden layer. The learning times and learning rate were set at 5000 and 0.02, respectively whereas the training accuracy was kept at  $1 \times 10^{-5}$ . The training process of the RBF neural network has been presented in Fig. 2. When 4 hidden layers were used, the number of training steps was 3820. However, the training steps were 4560 and 5000 when 3 and 5 hidden layers were employed, respectively. It was, therefore, concluded that the RBF neural network should contain 4 hidden layers with an overall network structure of  $3 \times 4 \times 1$ . Finally, the post-normalized data was calculated using Equation (3).

$$X_i = \frac{X - X_{\min}}{X_{\max} - X_{\min}} \quad (2)$$

$$X = X_{\min} + (X_{\max} - X_{\min}) \times X_i \quad (3)$$

where  $X$  and  $X_i$  represent pre- and post-normalized data, and  $X_{\max}$  and  $X_{\min}$  represent maximum and minimum values of the original data.

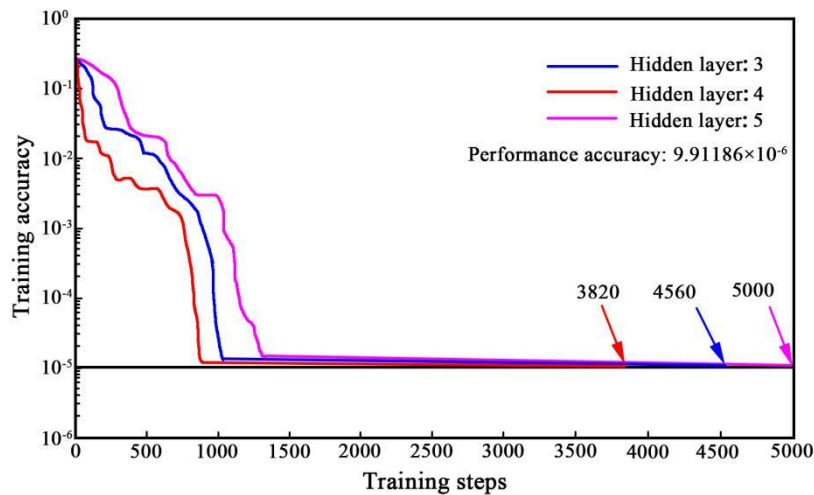


**Figure 2.** Training process of the RBF neural network

### 3.3 Predicted results from the RBF neural network

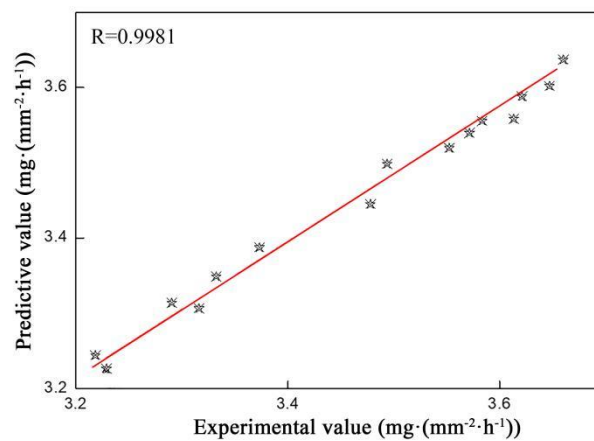
Table 3 and Fig. 3 show the results from the RBF neural network, and the agreement of results between experimental and predicted values. The fitting value ( $R$ ) for the RBF neural network employed was 0.9981, indicating that the RBF neural network used was suitable for predicting the corrosion rates of Ni-TiN composite coatings. In addition, the maximum and minimum errors of this neural network were 2.28% and 0.04%, respectively. This result implies that the RBF neural network employed here for predicting the corrosion rate of Ni-TiN composite coatings had an exceptionally high level of accuracy.

It has also been deduced from Table 3 that the minimum corrosion rate of Ni-TiN composite coatings was 3.214 mg/(mm<sup>2</sup>·h), and the serial number corresponding to the plating parameters employed was 9. Hence, the parameters for preparing Ni-TiN composite coatings are the following: a TiN concentration of 9 g/L, an electrolyte temperature equivalent to 45°C, and a current density of 0.6 A/dm<sup>2</sup>. In addition, the predicted corrosion rate of the coating obtained using the parameters listed in serial number 9 was 3.335 mg/(mm<sup>2</sup>·h), whereas the relative error was 0.04%. However, when the minimum predicted corrosion rate was 3.203 mg/(mm<sup>2</sup>·h), the relative error was up to 0.96%.

**Table 3.** Comparison between experimental and prediction values of RBF neural network

Serial number	Experimental value (Corrosion rate, mg·(mm <sup>2</sup> ·h <sup>-1</sup> ))	Prediction value (Corrosion rate, mg·(mm <sup>2</sup> ·h <sup>-1</sup> ))	Relative error (%)
1	3.629	3.546	2.28
2	3.586	3.551	0.97
3	3.231	3.367	1.08
4	3.478	3.445	0.95

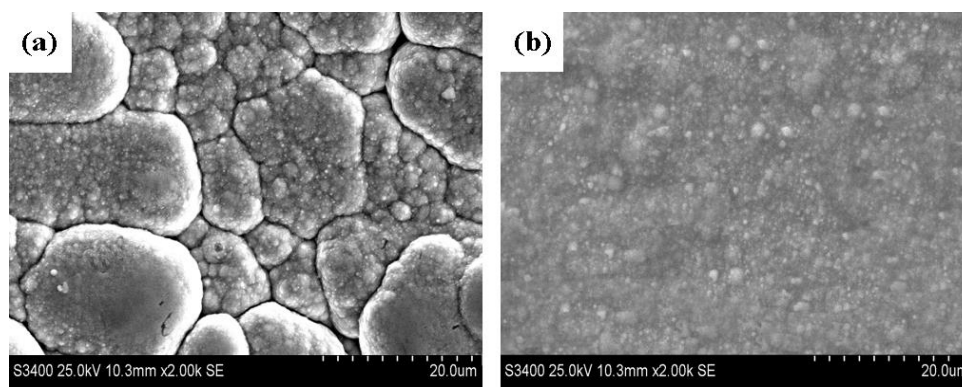
5	3.369	3.412	1.28
6	3.304	3.666	0.32
7	3.647	3.602	1.23
8	3.486	3.513	0.77
9	3.214	3.335	0.04
10	3.265	3.203	0.96
11	3.223	3.256	1.27
12	3.236	3.209	0.83
13	3.289	3.332	1.31
14	3.315	3.515	1.12
15	3.621	3.588	0.91
16	3.322	3.291	0.93



**Figure 3.** Fitting results between experimental and prediction values of RBF neural network

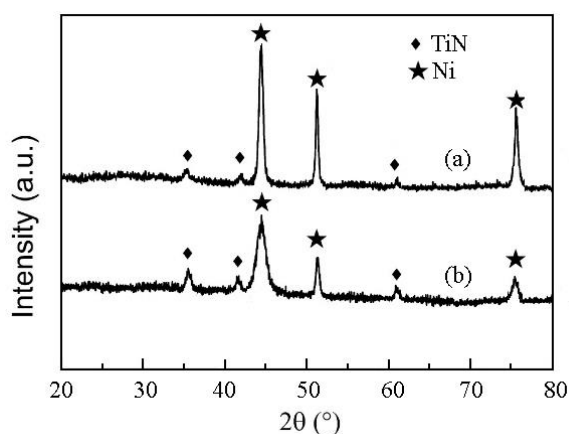
### 3.4 Characterization

To examine the results predicted from the RBF neural network, the parameters listed in serial numbers 1 and 9 were employed for manufacturing Ni-TiN composite coatings. The two sets of parameters were chosen based on the maximum and minimum experimental corrosion rates of Ni-TiN composite coatings. Fig. 4 shows the SEM images of Ni-TiN composite coatings obtained by using pulsed-current electrode deposition. A large surface undulation, coarse grain, and irregular microstructure emerged in the Ni-TiN composite coating, when a TiN concentration of 3 g/L was used, the bath temperature was kept at 45°C, and a current density of 0.2 A/dm<sup>2</sup> was employed. However, a flat, fine, and compact microstructure was observed in the Ni-TiN composite coating manufactured using a TiN concentration of 9 g/L, a bath temperature of 45°C, and a current density of 0.6 A/dm<sup>2</sup>. It was thus concluded that the appropriate choice of the process parameters can effectively inhibit the growth of Ni grains and promote the uniform distribution of TiN particles in coatings, resulting in the outstanding surface quality of Ni-TiN composite coatings [14].



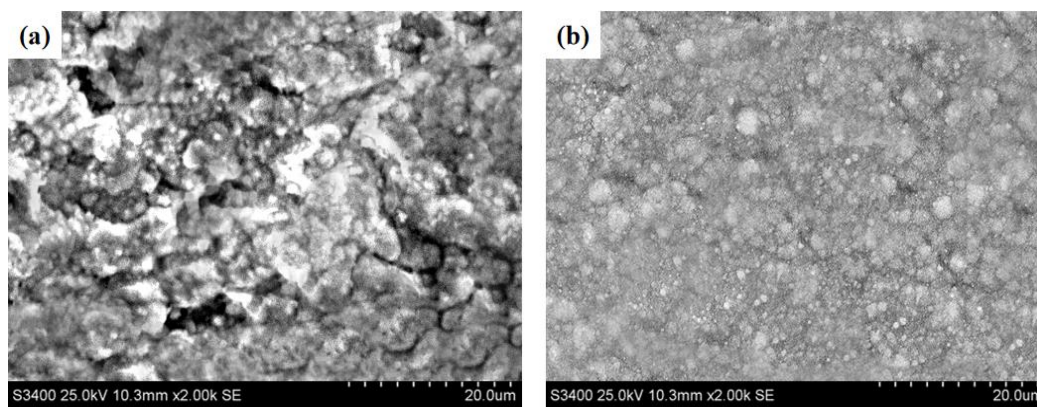
**Figure 4.** Surface morphologies of Ni-TiN composite coatings deposited at different parameters: (a) Serial number 1 (TiN concentration 3 g/L, bath temperature 45°C, current density 0.2 A/dm<sup>2</sup>, duty cycle 50%, plating time 45 min), (b) Serial number 9 (TiN concentration 9 g/L, bath temperature 45°C, current density 0.6 A/dm<sup>2</sup>, duty cycle 50%, plating time 45 min).

Fig. 5 shows the XRD patterns of Ni-TiN composite coatings. Ni and TiN phases were identified separately, in addition to the phase of the Ni-TiN composite coatings. The diffraction peak intensities from the TiN particles in the Ni-TiN composite coating deposited using the parameters mentioned in Serial number 9, were higher than that of the Ni-TiN composite coating obtained by using Serial number 1 parameters. In addition, the diffraction peak intensities of Ni grains in Ni-TiN composite coating deposited using the parameters listed in Serial number 9 parameters were lower and wider than that for Serial number 1 parameters, thereby indicating a finer microstructure obtained with Serial number 9 parameters. These results corroborate very well with SEM observations.



**Figure 5.** XRD patterns of Ni-TiN composite coatings deposited at different parameters: (a) Serial number 1 (TiN concentration 3 g/L, bath temperature 45°C, current density 0.2 A/dm<sup>2</sup>, duty cycle 50%, plating time 45 min), (b) Serial number 9 (TiN concentration 9 g/L, bath temperature 45°C, current density 0.6 A/dm<sup>2</sup>, duty cycle 50%, plating time 45 min).

Fig. 6 shows the SEM surface morphology of Ni-TiN composite coatings following corrosion. Obvious corrosion products were observed and large pits appeared on the surface of the Ni-TiN composite coating fabricated using a TiN concentration of 3 g/L, a bath temperature of 45°C, and a current density of 0.2 A/dm<sup>2</sup>. However, only a few corrosion products and pits emerged a TiN concentration of 9 g/L, a bath temperature of 45°C, and a current density of 0.6 A/dm<sup>2</sup> was used in the coating process.



**Figure 6.** Corrosion morphologies of Ni-TiN composite coatings deposited at different parameters: (a) Serial number 1 (TiN concentration 3 g/L, bath temperature 45°C, current density 0.2 A/dm<sup>2</sup>, duty cycle 50%, plating time 45 min), (b) Serial number 9 (TiN concentration 9 g/L, bath temperature 45°C, current density 0.6 A/dm<sup>2</sup>, duty cycle 50%, plating time 45 min).

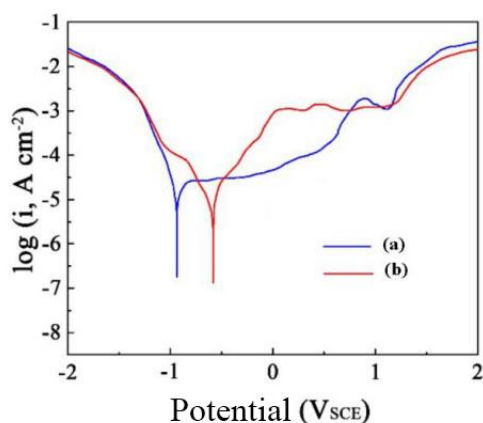


**Figure 7.** Polarization curves of Ni-TiN composite coatings deposited at different parameters: (a) Serial number 1 (TiN concentration 3 g/L, bath temperature 45°C, current density 0.2 A/dm<sup>2</sup>, duty cycle 50%, plating time 45 min), (b) Serial number 9 (TiN concentration 9 g/L, bath temperature 45°C, current density 0.6 A/dm<sup>2</sup>, duty cycle 50%, plating time 45 min).

Fig. 7 shows the polarization curves of the Ni-TiN composite coatings deposited at different parameters, and Table 4 presents the electrochemical corrosion data gathered from the potentiodynamic

polarization curves. The corrosion was strongest for Ni-TiN composite coatings obtained by using the parameters mentioned in Serial number 1, manifesting a corrosion potential of -0.925 V, whereas an outstanding corrosion resistance was observed when Serial number 9 parameters were employed in the process of coating.

The results presented here indicate that a fine and compact morphology of Ni-TiN composite coating, obtained by employing the parameters listed in Serial number 9, could effectively prevent the corrosion solution to invade the coating interior, thereby resulting in an improved corrosion resistance [15]. On the other hand, a rough structure of the coating leads to the corrosion solution easily entering into the interior of the nanocoating, thereby leading to an acceleration of the corrosion reaction which, in turn, is associated with poor corrosion resistance [16].

**Table 4.** Electrochemical corrosion parameters Ni-TiN composite coatings deposited at different parameters: Serial number 1 (TiN concentration 3 g/L, bath temperature 45°C, current density 0.2 A/dm<sup>2</sup>, duty cycle 50%, plating time 45 min), Serial number 9 (TiN concentration 9 g/L, bath temperature 45°C, current density 0.6 A/dm<sup>2</sup>, duty cycle 50%, plating time 45 min).

Serial number	Corrosion current (μA/cm <sup>2</sup> )	Corrosion potential (V)
1	52.491	-0.925
9	56.262	-0.593

#### 4. CONCLUSIONS

The main findings of this work can be summarized as follows:

(1) When 4 hidden layers were used in the RBF neural network, the total count of training steps was 3820. However, the training steps were respectively 4560 and 5000 when 3 and 5 hidden layers were used. Therefore, a total of 4 hidden layers of the RBF neural network result in optimum performance, with a total network structure of 3×4×1.

(2) The maximum and minimum errors of this neural network were 2.28% and 0.04%, respectively. This result demonstrated that the accuracy of the RBF neural network in predicting the corrosion rate of Ni-TiN composite coatings was exceptionally high.

(3) A flat, fine, and compact microstructure was observed for the Ni-TiN composite coating manufactured at a TiN concentration of 9 g/L, a bath temperature of 45°C, and a current density of 0.6 A/dm<sup>2</sup>. The diffraction peak intensities of Ni grains in the Ni-TiN composite coating deposited using the parameters listed in serial number 9, were lower and wider than that for using Serial number 1 parameters.

(4) The corrosion of Ni-TiN composite coating obtained by using Serial number 1 parameters was the strongest with a corrosion potential of -0.925 V, whereas the corrosion observed when using Serial number 9 parameters was the lowest, suggesting an outstanding corrosion resistance in the latter

case.

#### ACKNOWLEDGEMENT

This work has been supported by the National Natural Science Foundation of China (Guangxi Regional Foundation) (Granted no. 51965014), and the Guangxi Natural Science Foundation of China (Granted no. 2018GXNSFAA281306).

#### DATA AVAILABILITY

The data that support the findings of this study are available from the corresponding author upon reasonable request.

#### References

1. F. Xia, C. Li, C. Ma, Q. Li, and H. Xing, *Appl. Surf. Sci.*, 538 (2021) 148139.
2. M. Wu, W. Jia, and P. Lv, *Procedia. Eng.*, 174 (2017) 717-723.
3. C. Ma, G. Liang, Y. Zhu, H. Mu, and F. Xia, *Ceram. Int.*, 40 (2014) 3341-3346.
4. M. Winnicki, W. Apa, and Z. Znamirovski, *Coatings*, 11(2) (2021) 134.
5. F.F. Xia, W.C. Jia, C.Y. Ma, R. Yang, Y. Wang, and M. Potts, *Appl. Surf. Sci.*, 434 (2018) 228.
6. C. Ma, W. Yu, M. Jiang, and F. Xia, *Ceram. Int.*, 44 (5) (2018) 5163.
7. X.Y. Zhu and Z.C. Guo, *Adv. Mater. Res.*, 41-42(2008) 385-388.
8. Y. Liu, X. Han, L. Kang, B. Wang, X. Xiang, *Coatings*, 12(2) (2022) 145.
9. H. Liu, S. Ping, F. Zhang, X. Zhang, *Adv. Mater. Res.*, 791-793 (2013) 577-580.
10. Z. Yuan, L. Kong, D. Gao, X. Tong, S. Li, *Compos. Commun.*, 24 (1) (2021) 100671.
11. L. Wei, Y. Zhang, G. Liu, C. Ma, and W. Zheng, *Int. J. Electrochem. Sci.*, 16 (2021) 211017.
12. L. Li, B. Huang, G. Zhang, D. Wang, and C. Wang, *J. Cryst. Growth.*, 3 (2021) 126217.
13. A. Alexandridis, P. Patrinos, H. Sarimveis, and G. Tsekouras, *Chemometr. Intell Lab.*, 2 (2005) 149-162.
14. L. Yu, K.K. Lai, and S. Wang, *Neurocomputing*, 71(16-18) (2008) 3295-3302.
15. F. Xia, J. Tian, W. Wang, and Y. He, *Ceram. Int.*, 42(11) (2016) 13268-13272.
16. M.R. Vaezi, S.K. Sadrnezhad, and L. Nikzad, *Colloid. Surf. A.* 315 (2008) 176-182.

© 2022 The Authors. Published by ESG ([www.electrochemsci.org](http://www.electrochemsci.org)). This article is an open access article distributed under the terms and conditions of the Creative Commons Attribution license (<http://creativecommons.org/licenses/by/4.0/>).